Vortex Dynamics in Superconductors with a Triangular Array of Triangular Blind Antidots

B. Y. Zhu [a,b], L. Van Look [a], V. V. Moshchalkov [a], F. Marchesoni [b,c], and Franco Nori [b,d]

[a] *Laboratorium voor Vaste-Stoffysica en Magnetisme, Katholieke Universiteit Leuven, B-3001 Leuven, Belgium*

[b] *Frontier Research System, The Institute of Physical and Chemical Research (RIKEN), Wako-shi, Saitama 351-0198, Japan*

[c] *Istituto Nazionale di Fisica della Materia, Universitá di Camerino, I-62032 Camerino, Italy*

[d] *Center for Theoretical Physics, Physics Department, CSCS, University of Michigan, Ann Arbor, MI 48109-1120, USA*

Abstract

We report on numerical studies of the DC vortex transport properties, including V(I) curves and vortex trajectories, in triangular pinning arrays of triangular blind antidots. The asymmetric geometry of the pinning sites produces a significant influence on the vortex motion depending on the direction of the applied Lorentz force $\mathbf{F}_L$.

Key words: Vortex dynamics, Vortex pinning; Nonequilibrium dynamic vortex phases.

Asymmetric pinning [1–4] can be central to the design of superconducting devices. In this paper, we present numerical simulations of the motion of superconducting vortices interacting with a triangular array of triangular blind antidots. Here we focus on the DC vortex dynamics at opposite Lorentz force $\mathbf{F}_L$ orientations ($\mathbf{F}_L \parallel \mathbf{y}$ or $\mathbf{F}_L \parallel -\mathbf{y}$). A pronounced asymmetry in the dynamics, depending on the drive direction, has been found. The different constraint on the positions of the pinned vortices, when $\mathbf{F}_L$ is directed along opposite directions, leads to an asymmetric vortex depinning transition, which gives rise to the observed asymmetry in the dynamics.

We consider a blind antidot model for the triangular pinning traps. This means that no pinning force is exerted on the vortex once it is trapped inside the triangle. It also allows the possibility of a multiple-vortex occupancy of the pinning site, without the merging of the vortices into one multi-quanta vortex.

The pinning force of each triangular pinning center on a vortex is modelled as $\mathbf{F}_p(\mathbf{r}) = -F_{p0} f_0 \sum_{k=1}^{N_p} \mathbf{r}/R_p \exp\left(-|\mathbf{r}/R_p|^2\right)$, when the vortex is outside of the bottom area of the k^{th} triangular pinning center. Here, $\mathbf{r}$ is the distance between the vortex and the boundary of the k^{th} triangular pinning trap. $F_{p0} f_0$ denotes the strength of the individual pinning site force here fixed to $F_{p0} = 0.5$. The repulsive vortex-vortex interaction $\mathbf{F}_{vv}$ is modelled by the modified Bessel function K_1 [3]. The equation of motion is $\eta\mathbf{v} = \mathbf{F}_L + \mathbf{F}_{vv} + \mathbf{F}_p$. Here, $R_p = 0.4$, $\lambda = 6$, $\eta = 1$, and we fix the side length s_0 of the triangular pinning centers $s_0 \equiv \lambda/2 = a_0/2$, where a_0 is the spacing between pins.

Voltage-Current V(I) Characteristics and Vortex Flow Regimes. — Figure 1 shows $V(F_L)$ curves for $H/H_1 = 1.2$ for the applied driving force $\mathbf{F}_L$ directed along $+\mathbf{y}$ and $-\mathbf{y}$. Very asymmetric depinning transitions are obtained for the two opposite $\mathbf{F}_L$ orientations. For $\mathbf{F}_L \parallel -\mathbf{y}$, *a very single sharp jump* in the $V(F_L)$ curve is observed, indicating that *all* the vortices are suddenly depinned simultaneously at large drives. In contrast to this, for $\mathbf{F}_L \parallel \mathbf{y}$, we observe a *multi-stage depinning process* with initial depinning at a much lower F_L ($F_L \sim 0.14$). The vortex rows with the largest strain are first set in motion, while the commensurate rows stay pinned, see i.e., Fig. 2(a) and (b). With the gradual increase of the driving force, more and more incommensurate depinning transitions occur. The small jumps in the $V(F_L)$ curve around point c in Fig. 1 are due to the fact that all the forces

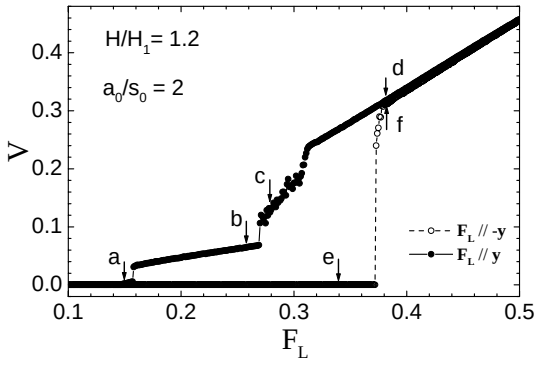

Fig. 1. Average vortex velocity V as a function of the driving Lorentz force for $\mathbf{F}_L$ directed along the positive and negative y-directions. The arrows and labels refer to the corresponding trajectories in Fig. 2(a)-(f).

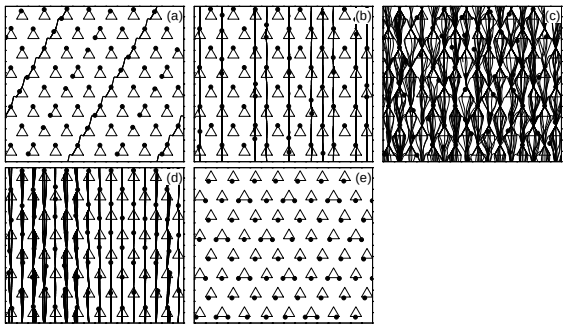

Fig. 2. (a)-(d): vortex trajectories at $F_L = 0.15$, 0.26, 0.28 and 0.38 for $\mathbf{F}_L$ directed along the positive $\mathbf{y}$-direction; (e)-(f): vortex trajectories at $F_L = 0.34$ and 0.38 for $\mathbf{F}_L$ directed along the negative $\mathbf{y}$-direction corresponding to the labels in figure 1.

barely balance and thus the moving vortices have many metastable states available and move left and right on the sample (see Fig. 2 (c)).

As seen in Fig. 2(e), two vortices can be easily accomodated inside the pinning trap when $\mathbf{F}_L \parallel -\mathbf{y}$. However, this is not possible when $\mathbf{F}_L \parallel \mathbf{y}$, because two trapped vortices tend to be driven to the upper corner pointing towards the positive y-direction. This greatly reduces the critical driving Lorentz force along $+\mathbf{y}$. This is the reason why a lower critical F_L^c value is obtained when $\mathbf{F}_L \parallel \mathbf{y}$ and a higher one in the case $\mathbf{F}_L \parallel -\mathbf{y}$.

Figure 2 (a)-(f) shows the pinning sites (open triangles), vortex positions (black dots) and vortex trajectories (lines) at $H/H_1 = 1.2$ for the different dynamic vortex phases indicated in Fig. 1. When $\mathbf{F}_L \parallel \mathbf{y}$ at $F_L = 0.15$ (Fig. 2(a)), most vortices are pinned and just a few move along "diagonal" trajectories. Fig. 2(a) also shows some fixed tilted columns that have two pinned vortices per trap. A reason that might trigger the motion of some diagonals versus others is the distance between triangular pins that have two trapped vortices in each triangle. Fig. 2(a) shows a pattern of inclined columns: 1) moving incommensurate inclined column; 2) pinned commensurate inclined column with one vortex per pin and 3) pinned matching inclined column with alternating one-two vortices per pin.

When the driving becomes strong enough, the vortices do not move diagonally anymore, but move straight up, as shown in Fig. 2(b). Again, commensurate vertical columns do not move (it costs relatively large energies to do so), while incommensurate ones do move. Since most of the vortices are depinned and move along the direction of the driving force in this case, there is a clear jump in the IV curve at $F_L \sim 0.16$ as seen in Fig.1 (filled circles). In Fig. 2(c) at $F_L = 0.28$, the driving force is sufficiently large and all the columns can be depinned. The V(I) curve is noisier in this phase than the two formers as seen in Fig. 1 (filled circles) because all the forces barely balance, each vortex has several metastable configurations to choose from and its motion oscillates "at random" (due to nearby vortices at a given time). In Fig. 2(d) all rows move orderly along the y-axis, but some rows appear to move faster than other ones. The more incommensurate the row, the easier it is to move.

When $\mathbf{F}_L \parallel -\mathbf{y}$, a different vortex behavior is revealed. In 2(e) at $F_L = 0.34$, the vortices are pinned with a pattern that somehow resembles the following (besides a few isolated defects): 1) horizontal row of pinned vortices with one vortex per pin (each pinned vortex located near the center of the south-facing side); 2) horizontal row of pinned vortices with alternating one-two vortices per pin (each pinned vortex located at the edges of the south-facing side). Of course, this configuration can hold the two vortices for a while, until the driving force is large enough, near $F_L \sim 0.38$ and the vortices suddenly move producing a sharp jump in the velocity and recovering the speed they had in (d). The columns with an incommensurate number of vortices move faster than the commensurate ones, which can be seen from the high number of trajectory lines in these columns.

This work was supported by the ESF Program "VORTEX", the bilateral BIL 00/02 China/Flanders Project, the Belgian IUAP, Flemish GOA and FWO Programs. BYZ and FN acknowledge support from the Frontier Research System of RIKEN, Japan and from the US National Science Foundation grant No. EIA-0130383.

References

[1] J. F. Wambaugh, *et al.*, Phys. Rev. Lett. **83**, 5106 (1999).

[2] C. J. Olson, *et al.*, Phys. Rev. Lett. **87**, 17700 (2001).

[3] B. Y. Zhu, *et al.*, Phys. Rev. B **64**, 012504 (2001).

[4] B. Y. Zhu, *et al.*, unpublished.